Construction and Building Materials 453 (2024) 139064

Contents lists available at ScienceDirect

Construction and Building Materials

journal homepage: www.elsevier.com/locate/conbuildmat

Effects of mix composition on the mechanical, physical and durability properties of alkali-activated calcined clay/slag concrete cured under ambient condition

Samuel De Carvalho Gomes [a], Quang Dieu Nguyen [a,*], Wengui Li [a,b], Arnaud Castel [a]

[a] School of Civil and Environmental Engineering, University of Technology Sydney (UTS), Sydney, NSW 2007, Australia

[b] Centre for Infrastructure Engineering and Safety, School of Civil and Environmental Engineering, The University of New South Wales, NSW 2052, Australia

ARTICLE INFO

Keywords:
Calcined clay
Slag
GGBFS
Alkali-activated concrete
Geopolymer
Chloride diffusion
Carbonation
MgO
pH
Potassium
KOH
Resistivity
XRD
chemical buffering
Superabsorbent Polymers (SAP)

ABSTRACT

Alkali-activated concrete (AAC), a possible alternative to ordinary Portland cement (OPC), provides increased environmental advantages, notably lower carbon emissions. Likewise, similar to OPC, it faces durability problems under severe environments. This study evaluated the effectiveness and durability of alkali-activated concretes containing low-grade calcined clay and granulated blast furnace slag (GGBFS), using NaOH/KOH as activators and MgO and superabsorbent polymer (SAP) as additives. The study's focus was on their physical-mechanical characteristics and performance under accelerated carbonation and chloride diffusion. Findings showed that calcined clay-GGBFS alkali-activated concretes exhibited a compressive strength range of 41.2–53.3 MPa, positioning them as a viable concrete for many structural usages. Nevertheless, the modified-RCPT (10 V) and NT Build 492 tests showed all concretes falling into the "high chloride penetrability" category, with values exceeding 350 coulombs and 13.5 ($\times 10^{-12}$ m^2/s) for the non-steady-state migration coefficient (D_{nssm}). NaOH and sodium silicate led to higher compressive strengths compared to KOH. Furthermore, the chloride migration coefficient of alkali-activated concrete blends ranged from 55.68 to 121.14 ($\times$ 10^{-12} m^2/s). The incorporation of 0.6 % SAP decreased compressive strength but improved the non-steady-state migration coefficient (D_{nssm}). Lastly, MgO-enriched samples showed the lowest water absorption and carbonation depth, attributed to the buffering action of magnesium phases, reducing carbonate formations, as revealed by XRD analysis.

1. Introduction

Traditional Portland cement-based concrete is a carbon intensive material due to the significant amount of carbon emissions from cement production [1]. One effective approach to addressing this issue is the reuse of recycled materials in concrete, which shows great potential for promoting sustainability and reducing waste. Although using recycled concrete aggregate can lead to a decrease in strength, the compressive strength values remain sufficient for engineering applications and the embodied energy value is noticeably reduced [2,3]. Another promising alternative is geopolymer concrete, also known as alkali-activated concrete, which offers a sustainable and environmentally friendly substitute for traditional Portland cement-based concrete. It is produced by combining industrial waste materials rich in aluminosilicates, such as fly ash or GGBFS with alkaline activators to form a binder that solidifies and hardens when mixed with aggregates [4,5]. The utilization of geopolymer materials in concrete production offers numerous environmental and economic benefits. By using geopolymer concrete, the carbon dioxide emissions associated with the manufacturing of cement can be significantly reduced. Furthermore, the use of industrial waste materials as a precursor for geopolymer binder helps to alleviate the burden of waste disposal and reduces the demand for natural resources [6]. Previous studies have utilized NaOH and KOH as the primary alkali solutions for synthesizing geopolymers. The presence of these metal ions in the solution has a distinct impact on both the geopolymerization reaction and the microstructural and structural properties [7]. Specifically, Na^+ ions derived from NaOH are preferred due to their smaller size, which enhances the rate of dissolution and facilitates better stabilization of silicate monomers and dimers within the solution. In contrast, K^+ ions possess a larger size compared to Na+, resulting in slower

* Corresponding author.
E-mail address: quangdieu.nguyen@uts.edu.au (Q.D. Nguyen).

https://doi.org/10.1016/j.conbuildmat.2024.139064
Received 26 July 2024; Received in revised form 16 October 2024; Accepted 4 November 2024
Available online 8 November 2024

condensation rates but still contribute to accelerating overall reaction kinetics.

Metakaolin, another aluminosilicate material used in the production of geopolymer concrete, is derived from the calcination of pure kaolinite clay. This process involves heating the clay at high temperatures to remove impurities and transform it into a reactive highly amorphous material. It is produced under closely monitored circumstances to enhance its physical characteristics, such as colour and particle size, with a significant purity and reactivity similar to pozzolanic materials [8]. However, the scarcity and high cost of high-purity kaolin clay have posed a challenge in its widespread use for concrete application. In order to address this issue, scholars and scientists have conducted investigations into alternative materials that can be used as substitutes for high-grade kaolin clay. One such material is low-grade calcined clays, which researchers are exploring as a potential solution to overcome the limitations caused by limited availability and elevated costs associated with traditional sources of kaolin clay [9,10].

Recently, there has been a growing interest in utilizing low-grade calcined clays as raw materials. These particular clays typically have a lower content of kaolinite [11,12]. Recent studies have demonstrated that these clays can be effectively integrated into geopolymers and cement concrete to serve as an abundant source of supplementary cementitious materials [13,14]. However, there has been limited research conducted on the mechanical performance and durability of these materials. The existing studies often lack a consensus in the literature due to variations in clay compositions and differences in evaluation parameters. Therefore, further investigation is required to establish clear guidelines for assessing the service life and durability of such materials [13,15].

The inclusion of precursors with significant proportion of calcium such as GGBFS in alkali- activated materials or low calcium fly ash geopolymer has been very promising in recent years [16]. Some recent studies have shown that the addition of calcium rich materials in Ca-free systems based metakaolin and calcined clay accelerates the setting time, its kinetic reactions and improves mechanical properties [17–19]. The findings suggest that the properties of the mortars are strongly influenced by the higher content of GGBFS, primarily because of its impact on Ca- rich phases like C-(A)-S-H/C-(N)-A-S-H calcium-aluminosilicate-hydrates. This promotes a denser microstructure and an increase in pH, as opposed to N-A-S-H which is typically found in geopolymer materials with low calcium content such as calcined clay and fly ash [17,20]. Most of these studies are using paste or mortar and focus only on the mechanical performance of the materials, resulting in a lack of information related to the durability of concretes based on the blend of calcined clay and GGBFS. Existing studies have not fully uncovered the mechanisms and potential improvements related to the long-term durability of alkali-activated materials (AAM). One important aspect that needs to be addressed is how AAMs withstand corrosion of steel reinforcement over time [21,22]. It is widely recognized that chloride ions are a major factor in causing the corrosion of steel reinforcement, which subsequently leads to the degradation of concrete structures. In addition, carbonation within the binding matrix has been found to lower the pH in pore solution. Therefore, it is crucial to investigate the resistance of alkali-activated materials to chloride ingress and carbonation to ensure their long-term durability [21]. Alkali-activated concrete, unlike ordinary Portland cement concrete, demonstrates reduced resistance to carbonation [21,23]. The factors that significantly influence the carbonation process in alkali-activated materials are generally acknowledged to be the type of precursor material used, the specific activators employed, the composition and concentration of ingredients utilized in its mixture design, along with the nature and abundance of alkali activators present. Moreover, parameters such as silicate modulus and existing conditions during carbonation also contribute extensively to determine how efficiently AAMs withstand this phenomenon [21].

Numerous research studies have indicated that reactive MgO exhibits the potential to serve as a substitute activator in order to enhance the resistance of alkali-activated materials against chloride intrusion [22,24,25] and carbonation [26–28], The inclusion of reactive MgO can lead to the formation of hydrotalcite-like phases through its hydration process, resulting in the formation of magnesium silicate hydrate, brucite and hydrotalcite ($Mg_6Al_2CO_3(OH)_{16}.4(H_2O)$) [26,29]. Hydrotalcite in alkali-activated materials have been identified to possess significant chloride adsorption capabilities attributed to their anion exchange capacity [22]. The addition of reactive MgO has been observed to have a beneficial effect on the formation and reduction of degradation rates of C-(A)-S-H gel. As a result, this enhancement plays a significant role in improving the resistance to carbonation in alkali-activated slag binders [22].

In addition to magnesium oxide, there has been increasing interest in the use of superabsorbent polymers (SAP) as internal curing agents in alkali-activated materials [30]. These SAPs have gained attention due to their ability to absorb and retain water, which helps mitigate issues such as shrinkage and cracking that can occur during the hydration process. By incorporating SAPs into alkali-activated systems, it is possible to provide a steady supply of moisture throughout the material, promoting more uniform hydration and improving overall durability. The inclusion of SAPs offers an innovative solution for enhancing the performance characteristics of these materials [31]. In a recent study by Al Makhadmeh and Soliman [31], the utilization of SAPs in alkali-activated slag-based systems was investigated. The research determined that an optimal dosage of 0.6 % of SAPs resulted in shrinkage reduction and increased hydration degree. Additionally, this optimal dosage also contributed to improvements in surface quality and anti-permeability properties.

Although the effects KOH activator, MgO and SAP have been evaluated in previous studies on alkali-activated materials using fly ash or GGBFS, a research gap remains in understanding the properties of alkali-activated calcined clay and GGBFS when using KOH, MgO and SAP in the mix composition. Therefore, this study investigated the performance of alkali-activated concretes composed of a low-grade calcined clay and GGBFS, with various activators (NaOH/KOH) as well as additives such as MgO and SAP. The focus was on examining the physical-mechanical properties, including their resistance to accelerated carbonation and chloride diffusion. Furthermore, at the time of submission, to the best of the authors' knowledge, no prior research has been conducted on investigating the impact of KOH, MgO, and SAP on the accelerated carbonation and chloride diffusion of alkali-activated concrete incorporating calcined clay and GGBFS.

2. Materials and mix compositions

2.1. Raw materials

The calcined clay obtained from Argeco was produced using an advanced industrial flash calcination method in France. With a kaolinite content of 55 wt%, this calcined clay falls under the category of low-grade clays. The GGBFS used in the study was supplied by Australian Steel Mill Services, based in Port Kembla, New South Wales, Australia. The magnesium oxide (MgO) used in this research was obtained from Chem-Supply Australia and had a purity level of 96 %. A white, free-flowing type of superabsorbent polymer (SAP) was employed in the experiment. This SAP has a remarkable capacity to absorb and retain liquid up to 500 times its own weight. The chemical compositions of calcined clay and GGBFS were measured by X-ray Fluorescence (XRF) in Table 1. The crystalline phases of the calcined clay, GGBFS and MgO are presented on Fig. 1, which is basically constituted of calcite, quartz, kaolinite, zeolite and periclase (MgO). The alkaline activator for the calcined clay-GGBFS alkali-activated concrete was composed by mixing sodium silicate solution ($Na_2O = 9.1$ %, $SiO_2 = 28.9$ % and Weight Ratio (SiO_2:Na_2O) 3.16–3.26) with sodium hydroxide (NaOH) pellets (purity: 98 %, specific gravity: 2.13 g/cm^3, pH: 14) for most of the mixes. Two of

Table 1
Chemical compositions of Calcined clay and GGBFS.

Chemical composition	Calcined clay (wt%)	GGBFS (wt%)
SiO_2	70.42	31.52
Al_2O_3	22.34	12.22
Fe_2O_3	2.34	1.14
CaO	0.49	44.53
MgO	0.16	4.62
Na_2O	0.1	0.21
K_2O	0.19	0.33
TiO_2	1.1	1.03
SO_3	0.02	3.24
Loss on ignition (LOI)	1.76	0.79

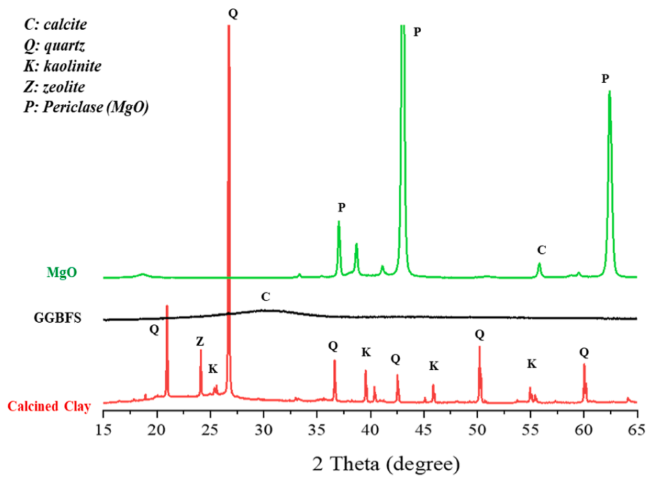

Fig. 1. XRD patterns of Calcined clay, GGBFS and MgO.

the mixtures were modified by replacing sodium hydroxide with potassium hydroxide (KOH) (purity: 98 %, specific gravity: 2.04 g/cm^3, pH: 14). The sand has a specific gravity of 2.65 and water absorption of 3.5 % while the coarse aggregate (10 mm basalt) has water absorption of 1.79 %. The crushing index value of basalt is less than 20 %, complying with Australian Standard AS 2758.1. The aggregates in this study are commercially available and commonly used for producing OPC-based concretes. Both coarse and fine aggregates were kept in sealed bulk bags to prevent contamination. The moisture content of the aggregates was measured before mixing to adjust the water content and achieve the saturated surface dry (SSD) condition.

2.2. Alkali-activated concrete mix compositions

The alkali-activated concrete mixtures were formulated in accordance with Table 2, using the optimal ratios of calcined clays and GGBFS identified in the previous study of the authors [20]. An alkaline solution with a Na_2O/binder of 10 % and a modulus ratio (Ms = SiO_2/Na_2O molar ratio) equal to 1.5 was created for the first six mix compositions in Table 2, as indicated by "N. The last two mixtures substituting NaOH pellets by KOH pellets, denoted by "K" (Table 2). The activator solution was prepared 24 h prior to usage. To assess the influence of SAP on the mixture, 0.6 % SAP/solid was added to the mixture. Additionally, in order to compensate for this addition of SAP, water/solid ratio was increased to 0.53 in 70CC30S-NS and 50CC50S-NS to maintain the same workability [31]. In addition, 5 % GGBFS was replaced by reactive MgO and labeled as “NM” in two mix designs in Table 2. This ratio was determined to be optimal based on previous studies aimed at enhancing the resistance of alkali-activated concrete against chloride penetration and carbonation [22]. The samples were mixed in an electric Pan-drum mixer. Afterwards, fresh concrete was poured into 100 mm × 200 mm cylindrical moulds and vibrated on a vibrating table to remove trapped air. After one day, all concrete samples were demoulded, sealed to prevent moisture loss and transferred to a controlled room with a temperature of 23 ± 2 °C until testing.

3. Experimental program

3.1. Compressive strength

The compressive strength of the calcined clay-GGBFS alkali activated concrete was measured at 28 days, using three cylinders according to ASTM C39 [32]. The compression testing was conducted using a Universal Hydraulic Test Frame UH-500kN XR at the loading rate of 0.25 MPa/s ± 0.05 MPa/s. The samples were wrapped and sealed one day after casting and cured for 28 days in the controlled room at a constant temperature of 23 ± 2°C and 55 % relative humidity until they were tested.

3.2. The water absorption and volume of permeable voids (VPV)

The water absorption and permeable void volume tests were conducted on disc specimens with a diameter of 100 mm and a thickness of 50 mm. These discs were obtained by cutting standard cylinders, ensuring that the sampling location was at least 25 mm away from both the top and bottom faces of the cylinders. The samples were first dried in an oven at a temperature of 105°C for approximately 48 hours or until there was no significant change in weight (mass change <0.5 %) within a period of 24 hours [33]. The measurement of water absorption and

Table 2
Alkali-activated concrete experimental design mixes.

Mixing(1)	GGBFS (%)	Activator modulus (Ms)(2)	(Na_2O+K_2O)/binder (%)(3)	Total Binder (kg/m^3)	Coarse/Fine aggregate ratio	Water/Solid(4)
70CC30S-N	30	1.5	10	400	1.9	0.45
50CC50S-N	50	1.5	10	400	1.9	0.45
70CC30S-NS(5)	30	1.5	10	400	1.9	0.53
50CC50S-NS(5)	50	1.5	10	400	1.9	0.53
70CC30S-NM(6)	25	1.5	10	400	1.9	0.45
50CC50S-NM(6)	45	1.5	10	400	1.9	0.45
70CC30S-K(7)	30	1.5	10	400	1.9	0.45
50CC50S-K(7)	50	1.5	10	400	1.9	0.45

*Note 1: CC: Calcined clay, S: GGBFS. The numeric value preceding the acronym indicates the proportion of the precursor in the mixture.
*Note 2: Ms = $SiO_2/(Na_2O + K_2O)$
*Note 3: Binder = Calcined clay + GGBFS + reactive MgO
*Note 4: Water: free water + water in silicate solution. Solid: Binder + solid in silicate solution (SiO_2 and Na_2O) + NaOH/KOH pellets
*Note 5: 0.6 % SAP/solid
*Note 6: 5 % of GGBFS was replaced by reactive MgO referred to as "NM" for simplicity.
*Note 7: NaOH pellets were replaced by KOH pellets

volume of permeable voids (VPV) in the concrete after 28 days was conducted by using ASTM C642 [34].

3.3. Chloride diffusion tests: modified RCPT-10V and NT Build 492

To determine the resistance of concrete to the penetration of chloride ions, a rapid chloride penetration test (modified RCPT with 10 V of voltage) proposed by Noushini and Castel [35] was applied. The normal voltage of 60 V in RCPT-ASTM C1202 [36] could not be used due to the high conductivity of the samples resulting in overheating [35]. The rapid chloride permeability test was carried out on three identical companion specimens after 28 days of curing. The samples used for testing had a thickness of 50 mm and a diameter of 100 mm.

In order to determine the chloride migration coefficient under non-steady-state conditions, the chloride migration test was conducted in accordance with the Nordtest NT Build 492 test method [37]. The samples consisted of 50-mm-thick concrete discs that were cut from the middle portion of three identical cylinders measuring 100×200 mm after 28 days of casting. For conducting the experiment, a catholyte solution containing 10 % NaCl in tap water and an anolyte solution comprising of 0.3-N NaOH in distilled water were utilized. To determine the chloride penetration depth in saturated specimens, an axial potential ranging from 10 to 60 V was applied. This electric field induces migration of chloride ions from outside the specimen into its interior. After a specific duration (ranging from 6 to 24 hours), the specimen is split axially into two parts. To measure the penetration depth accurately, an $AgNO_3$ solution with a concentration of 0.1 mol/L is sprayed on the cross-section of each half. By following NT Build 492 guidelines [37], the non-steady-state migration coefficients were calculated.

3.4. Surface and bulk resistivity

The measurements of both surface and bulk resistivity were conducted at 28 days by utilizing a Proceq Resipod resistivity measuring instrument (Fig. 2). Cylindrical samples with dimensions of 100 × 200 mm were vacuum saturated with water. The surface resistivity of the specimens was assessed using the Proceq Resipod device with a four-pin Wenner probe array extension. The spacing between the electrodes on the probe array extension was set at 50 mm. Twelve measurements were conducted for each specimen, with four measurements taken at intervals of 90° around the specimen [38]. The measurement of bulk electrical resistivity was conducted using the Proceq Resipod device, whereby two stainless steel contact base plates were connected [33].

3.5. Accelerated carbonation test

Accelerated carbonation test was performed using samples of 50 mm thick concrete discs cut from the middle part of three identical 100 × 200 mm cylinders. The samples were sealed one day after casting and cured for 28 days, then the samples were unsealed and stored for two weeks in a controlled room at a constant temperature of 23 ± 2°C and 55 % relative humidity until transferred to the carbonation chamber. For accelerated carbonation, specimens were placed in a carbonation chamber at 2 % CO_2 concentration, 23°C and 55 % relative humidity. To restrict the diffusion of CO_2 to only the top and bottom surfaces, self-adhesive aluminum foil was securely applied around the circumference of the disc. After 2 and 8 weeks of exposure, the carbonation depth was measured by applying 1 % solution of phenolphthalein in alcohol to the surface of the split concrete specimens. For the accelerated carbonation test, two OPC concretes with 40 % replacement of OPC by GGBFS were prepared for comparison. The first one called OPC-S50 (50 MPa grade) and the second one OPC-S40 (40 MPa grade). The two mixes were submitted to the same conditions as the alkali activated concretes.

Fig. 2. Bulk resistivity (a) and surface resistivity (b) measurement.

3.6. pH measurements

The pH of the hardened alkali-activated pastes was determined after 28 days of curing. Paste mixes were prepared according to the proportions specified in Table 2, but without including any aggregate. In order to carry out this measurement, crushed and ground paste samples were obtained by passing them through a sieve with a size of 75 µm. These ground paste samples were then dispersed in distilled water at a ratio of 1:1 and mixed for a duration of five minutes [39,40]. The pH value was measured using a pH meter with an accuracy level of ±0.01 and three separate measurements were taken.

3.7. X-ray diffraction (XRD) analysis

The mineralogical composition of the composite material was determined using X-ray diffraction analysis after 28 days (uncarbonated) and 8 weeks of accelerated carbonation. The analysis was carried out with a Bruker D8 Discover diffractometer, using a fine powder paste obtained from paste samples aged for 28 days and subjected to carbonation for 8 weeks. The concrete powder was sieved through 75 µm size prior to XRD analysis. The XRD measurements were performed at an electrical current of 20 mA and voltage of 40 kV, scanning within a range of 2θ angles from 5° to 80°.

4. Results and discussion

4.1. Compressive Strength

The compressive strengths of the concrete made from alkali-activated calcined clay and GGBFS, which were sealed and cured at a temperature of 23 ± 2°C for a duration of 28 days, are illustrated in Fig. 3. Overall, the calcined clay-GGBFS geopolymer concretes exhibited an average compressive strength between 41.2 and 53.3 MPa. This performance qualifies them for a broad range of structural uses, even in challenging environmental conditions. According to Australian Standards AS 3600 and AS 5100 [41,42], these compressive strength values indicate that alkali-activated calcined clay and GGBFS concretes are suitable for A, B1 and B2 exposure classifications, including interior and exterior environments. The analysis was organized into groups according to the ratio of calcined clay and GGBFS precursors.

For the samples containing 70 % calcined clay and 30 % GGBFS (70CC30S group), it is evident that the mixture with NaOH without any additional substances (70CC30S-N) exhibited the highest compressive strength (50.7 MPa). On the other hand, the lowest compressive strength was observed for the mixture consisting of NaOH along with an addition of SAP (41.2 MPa). Fig. 3 shows the compressive strength results varied for different the mixtures containing 50 % calcined clay and 50 % GGBFS (50CC50S group). Similar to 70CC30S group, the mixture

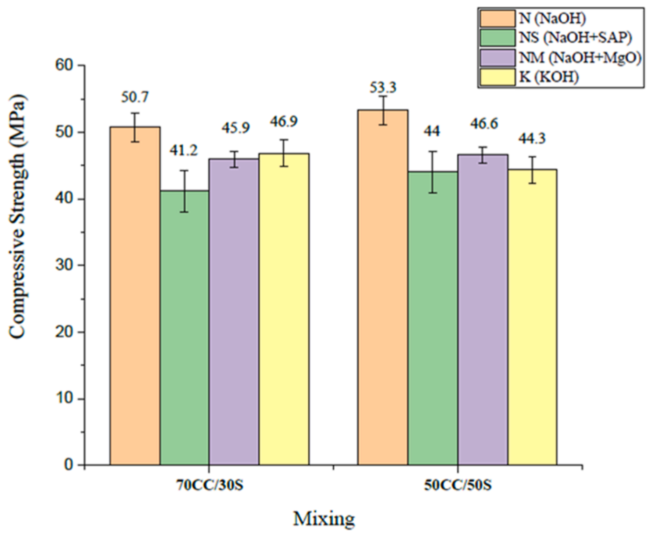

Fig. 3. Compressive strength of alkali-activated calcined clay/GGBFS concrete blend.

identified as 50CC50S-N exhibited the highest compressive strength of 53.3 MPa, indicating its superior performance compared to other combinations. In contrast, specimens with KOH as the activator (50CC50S-K) showed lower compressive strengths at approximately 44.3 MPa. In previous studies, researchers [43,44] have conducted comparisons between different activators and found that sodium hydroxide performed better than potassium hydroxide when the specimens were cured at room temperature. NaOH possesses a more effective capacity to dissolve minerals compared to KOH at equivalent concentrations [45]. Furthermore, it has been observed that K-A-S-H (alkaline aluminium silicate hydrate gel) exhibits a higher degree of chemical instability than N-A-S-H (activated with NaOH) gel [46,47]. This characteristic of K-geopolymers could potentially account for their lower compressive strength values in comparison to Na-geopolymers [48,49]. However, replacing NaOH by KOH can provide the better chloride resistance as presented in Section 4.3.

The addition of 5 % magnesium oxide slightly decreases the compression strength of the mixtures when compared to NaOH-activated blends (70CC30S-N and 50CC50S-N), where 70CC30S-NM and 50CC50S-NM showed around 9.47 % and 12.57 % reduction in compression strength. The reason for this difference in strength could be attributed to the substitution of GGBFS with MgO, which results in hydrated products that are not as robust as the C-A-S-H formed through GGBFS activation. The reaction products due to the presence of MgO can be hydrotalcite, brucite and unreacted MgO [39,50]. The details of different reaction products are thoroughly discussed in Section 4.7. The greatest decrease was observed for the specimens that incorporated 0.6 % SAP into their composition (70CC30S-NS and 50CC50S-NS). Aside from the advantages associated with internal curing and shrinkage reduction, the addition of extra water to account for SAP absorption and the presence of macro voids in pastes containing SAP, contribute to a decrease in compressive strength [51,52]. Fig. 4 shows the macro voids in alkali-activated paste generated by SAP in 50CC50S-NS and 70CC30S-NS mixtures. The mechanism behind this phenomenon has been extensively investigated in studies involving the addition of SAP to both cement pastes and alkali- activated GGBFS materials [52–54]. Despite the slight reduction in compressive strength, the positive effects of adding SAP on other properties of alkali-activated calcined clay and GGBFS are discussed in the following sections.

4.2. The water absorption and volume of permeable voids (VPV)

The water absorption and volume of permeable voids (VPV) of the alkali-activated concrete specimens was carried out as one of the indicators for the durability properties. Table 3 shows the water absorption of the activated alkali concretes. When magnesium oxide was incorporated into the specimens (70CC30S-NM and 50CC50S-NM), they exhibited the lowest water absorption levels, achieving approximately 6.9 % and 6.6 %, respectively. Conversely, when SAP were added to the samples (70CC30S-NS and 50CC50S-NS), their water absorption increased significantly and reached values of approximately 7.79 % and 8.44 %, respectively. The inclusion of reactive MgO in the samples resulted in a decrease in water absorption, even though their compressive strength (Fig. 3) was lower compared to the samples with no replacement of GGBFS (70CC30S-N and 50CC50S-N). A similar finding was reported by Suescum-Morales et al. [50], who studied the effects of MgO and fly ash on hydration products. This addition led to the formation of hydrotalcite and brucite, which had the ability to fill voids and capillaries, thus limiting water accessibility. Although the presence of hydrotalcite and brucite decreased the water absorption and VPV (Table 3), hydrotalcite and brucite are considered as weak and expansive reaction products [55,56], leading to volume metric instability and reduction in compressive strength, as shown in Fig. 3.

The VPV exhibits the same trends as the water absorption (Table 3), where the samples activated with NaOH without any addition

Table 3
Water absorption and volume of permeable voids (VPV) of alkali-activated Calcined clay/ GGBFS concrete blend.

Mix	Water Absorption (%)	VPV (%)
70CC30S-N	7.298 (± 0.12)	17.70 (± 0.23)
70CC30S-NS	7.785 (± 0.42)	18.09 (±0.83)
70CC30S-NM	6.941 (± 0.11)	17.34 (± 0.13)
70CC30S-K	7.486 (± 0.11)	17.66 (± 0.19)
50CC50S-N	7.059 (± 0.15)	16.47 (± 0.11)
50CC50S-NS	8.443 (± 0.83)	18.62 (± 0.66)
50CC50S-NM	6.604 (± 0.07)	16.14 (± 0.16)
50CC50S-K	7.205 (± 0.19)	16.68 (± 0.23)

Fig. 4. Macro voids generated by SAP alkali-activated Calcined clay/ GGBFS paste blend.

(70CC30S-N and 50CC50S-N) demonstrated similar values to those activated with KOH. Furthermore, the specimens that incorporated reactive magnesium exhibited the lowest measured values, whereas those incorporating SAP demonstrated the highest recorded values. In the majority of the mixtures examined, it was found that a higher percentage of GGBFS resulted in lower water absorption and volume of permeable voids. Specifically, specimens with 50 % GGBFS (50CC50S-group) consistently exhibited lower values compared to those with 30 % GGBFS or less (70CC30S- group). However, an interesting exception was observed in mixtures containing SAP, as both water absorption and VPV were found to have higher values for the 50CC50S-NS mixture when compared to the 70CC30S-NS mixture. It is important to mention that the mixtures with a composition of 50CC50S-NS exhibited the presence of noticeable, white-colored products formed in the larger voids surrounding the desorbed hydrogel paste (Fig. 4). However, this phenomenon was not observed in pastes/concretes containing a higher proportion of calcined clay (70CC30S-NS).

4.3. Rapid chloride penetration test (modified RCPT-10V)

To measure the chloride penetration resistance of alkali-activated concrete mixes, an RCPT test (modified with 10 V) was performed, and the results of the RCPT test are shown in Fig. 5. Charges passed in Coulombs for the 70CC30S-N, 70CC30S-NS, 70CC30S-NM, 70CC30S-K mixtures were observed at 1105.3, 1234.5, 1108, and 977.3 Coulombs, respectively. Mixtures with 70 % of calcined clay and activated with KOH (70CC30S-K) obtained lower values of RCPT compared to 70CC30S-N. A similar pattern was noted on Fig. 5 for the specimens of the 50CC50S group. However, specimens activated with sodium hydroxide displayed slightly better outcomes than those activated with KOH. This indicates that KOH had a more significant effect on chloride resistance of alkali-activated concretes containing more calcined clay (70CC30S) compared to 50CC50S concretes. This trend changed when SAP was introduced, as specimens mixed with SAP (50CC/50S-NS) exhibited the highest recorded electrical charge of 1458 Coulombs. The replacement of GGBFS by 5 % of MgO did not show a considerable impact on the concrete performance.

For all the combinations, the species with the highest content of calcined clay (70CC30S- group) obtained lower and better results comparing to the mixtures with only 50 % calcined clay (50CC50S-group). As the previous research of the authors [20] has shown, increasing the amount of calcined clay relative to GGBFS leads to a dominant phase of N-A-S-H over C-A-S-H. The presence of free Na^{+} in the pore solution will undergo counter-diffusion when an electrical field gradient is imposed, causing Cl^{-} ions to move through the pore network and possibly overestimating the chlorides passing [16]. An elevated production of N-A-S-H due to the increase of calcined clay in the binder contributes to a decrease in the concentration of free Na^{+} present in the pore solution, consequently reducing the overall amount of charge passed. In addition, based on the proposal by Noushini and Castel [35] for the modified version of RCPT using 10 V and the correlation of the ASTM C1556 [57] chloride diffusion test results, all eight mixes (Fig. 5) would be classified as "High Chloride penetrability" due to the charge passed for the modified ASTM C1202 [58] being superior to 350 coulombs.

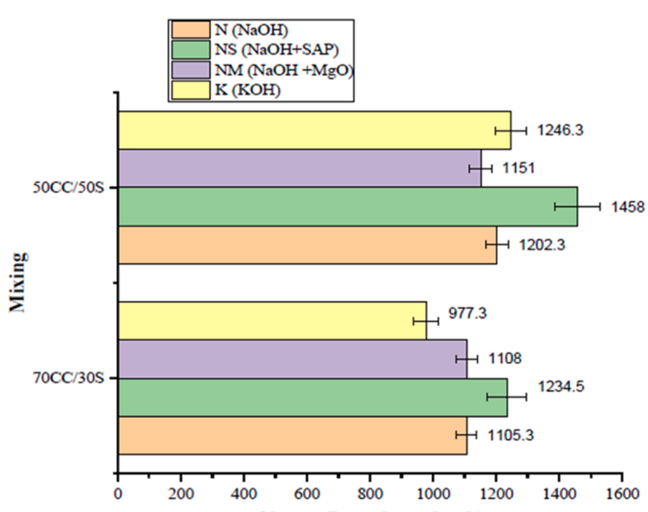

Fig. 5. Modified RCPT of the Alkali-activated concrete mixes.

4.4. Rapid migration test (RMT) - NT BUILD 492

The results in Table 4 presents the non-steady-state migration coefficient (D_{nssm}) of all concrete mixes. The D_{nssm} values ranged between 55.68 and 121.14 ($\times 10^{-12}$ m^2/s). Among the samples containing 50 % calcined clay and 50 % GGBFS (50CC50S- group), the best outcome was achieved by the mixture labeled as 50CC50S-N that was activated only with NaOH and sodium silicate without any additional substance. This particular sample yielded a result of 55.68 $\times$ 10^{-12} m^2/s. On the other hand, when MgO was added to the 50CC50S-NM mix or when KOH (50CC50S-K) was used as activator, higher results were obtained at values of 98.46 and 97.30 $\times$ 10^{-12} m^2/s respectively. Replacing GGBFS with MgO resulted in a decrease in the ability to resist chloride penetration. Unlike previous studies where adding 5 % was enough to generate hydrotalcite-type phase and subsequently improve resistance against chloride attack [25,59], no advantageous effect against chloride diffusion was observed when using MgO in calcined clay-GGBFS alkali-activated concretes. In addition to its higher water absorption and VPV outcomes when compared to an equivalent quantity of the precursor, 50CC50S-NS with SAP yielded a moderate value of 77.80 $\times$ 10^{12} m^2/s in comparison to the others. In general, increasing the amount of C-A-S-H gel in alkali-activated materials has been found to lower porosity and improve resistance to chloride penetration. The calcium content of the precursors plays a significant role in determining the mechanical properties and chloride-resistant capabilities of alkali-activate concretes [21].

The mixture labeled as 70CC30S-NS displayed the most favorable outcome when comparing mixtures with a composition of 70 % calcined clay and 30 % GGBFS (Table 4). This particular combination showed superior performance when activated with NaOH and incorporating 0.6 % SAP. The inclusion of SAP resulted in a decrease in the depth of penetration, as shown by Fig. 6, compared to the sample without SAP. The reduction achieved was around 20.4 % in comparison to 70CC30S-N. The chloride migration coefficient of 70CC30S-N and 70CC30S-K showed almost identical performance, indicating that the type of alkaline activator used had minimal impact on their resistance to chloride migration. Moreover, substituting GGBFS with 5 % MgO did not significantly affect the results either. It is noteworthy that among all the mixtures tested, 70CC30S-NM exhibited the highest D_{nssm} value at approximately 121.14 $\times$ 10^{-12} m^2/s. In agreement to the modified-RCPT

Table 4
Non-steady-state migration coefficient (D_{nssm}) of alkali-activated concretes after 28 days.

Mixes	NT Build 492	
	Applied voltage (V)	D_{nssm} ($\times$ 10^{-12} m^2/s)
70CC30S-N	10	116.74 ($\pm$ 7.83)
70CC30S-NS	10	92.91 ($\pm$ 8.58)
70CC30S-NM	10	121.14 ($\pm$ 9.17)
70CC30S-K	10	118.26 ($\pm$ 5.23)
50CC50S-N	10	55.68 ($\pm$ 6.10)
50CC50S-NS	10	77.80 ($\pm$ 2.64)
50CC50S-NM	10	98.46 ($\pm$ 10.01)
50CC50S-K	10	97.30 ($\pm$ 7.22)

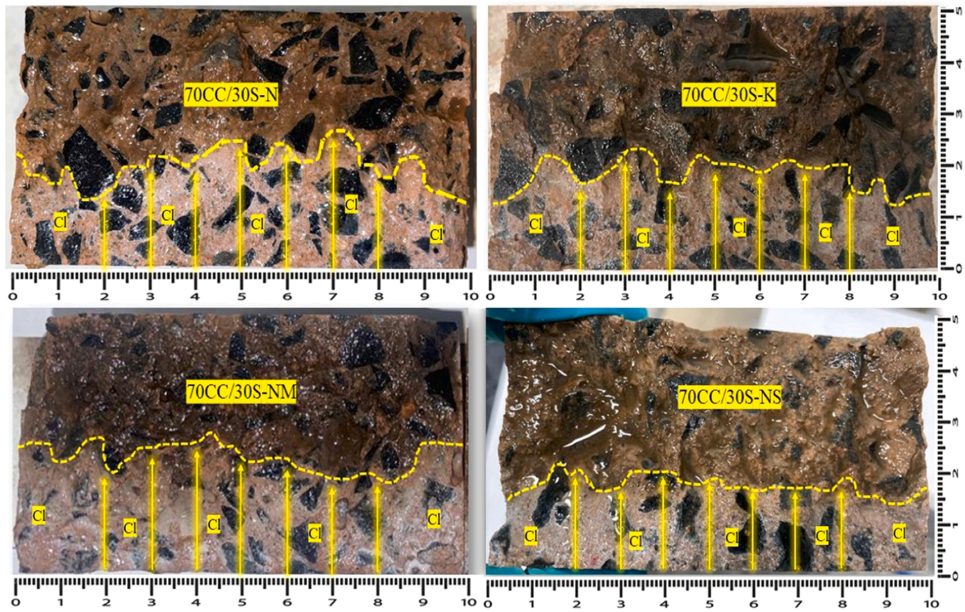

Fig. 6. Chloride Penetration Depth measurement after conducting NT Build 492.

results and based on the proposal by Noushini et al. [60] for the alkali-activated concrete performance in chloride environments using NT Build 492 and the correlation of ASTM C1556 [37,57], the non-steady-state migration coefficient (D_{nssm}) of all concrete mixes (Table 4) would be classified as "High Chloride penetrability" due to its value being higher than 13.5 $\times 10^{-12}$ m^2/s, and not recommended for chloride environments.

4.5. Surface and bulk resistivity

The resistivity of concrete is widely recognized as a dependable measure of its ability to withstand the penetration of aggressive ions such as Cl^- and CO_2 [38]. It serves as an indicator for the level of resistance that concrete exhibits against the flow of ionic currents within its pore solution. Concrete with lower porosity and higher tortuosity restricts the movement of ions like Na^+, K^+, and OH^- in the pore solution [33]. Consequently, higher electrical resistivity signifies reduced permeability, while lower electrical resistivity indicates greater permeability [38]. An additional significant factor to consider is the quantity of metallic ions present in the pore solution. In substantial quantities, these ions have a detrimental effect on surface resistivity by diminishing it [61]. According to Table 5, the concrete surface and bulk resistivity of the 70CC/30S-N and 50CC50S-N mixtures were found to be slightly greater compared to the other containing the same combination of precursor materials. The bulk resistivity values observed were 2.33 kΩ.cm and 2.11 kΩ.cm respectively, while the corresponding values for the surface resistivity were found to be 5.91 kΩ.cm and 5.25 kΩ.cm. Meanwhile, the mixtures activated with KOH (70CC30S-K and 50CC50S-K) obtained the lowest values for bulk and surface resistivity, which is probably associated with a high concentration of K^+ free in the pore solution and a higher porosity based on the results of water absorption and VPV (Table 5).

Table 5
Surface and bulk resistivity of alkali-activated concrete after 28 days.

Mix Reference	Bulk resistivity (kΩ.cm)	Surface resistivity (kΩ.cm)
70CC/30S-N	2.33 (± 0.08)	5.91 (± 0.23)
70CC/30S-NS	2.01 (± 0.08)	4.63 (± 0.17)
70CC/30S-NM	2.13 (± 0.04)	5.48 (± 0.19)
70CC/30S-K	1.85 (± 0.11)	4.83 (± 0.11)
50CC/50S-N	2.11 (± 0.12)	5.25(± 0.25)
50CC/50S-NS	2.09 (± 0.11)	5.08 (± 0.24)
50CC/50S-NM	1.85 (± 0.06)	4.41 (± 0.21)
50CC/50S-K	1.66 (± 0.07)	4.18 (± 0.18)

Except for mixtures containing SAP, the performance of mixtures group 70CC30S was superior when compared to their corresponding counterparts with a composition ratio of 50CC50S. This observation is consistent with the findings from the modified RCPT-10V, where the mixtures containing a higher proportion of calcined clay (70CC30S-) exhibited superior performance. This improved behavior can be attributed to a possible reduction in the concentration of free sodium ions (Na^+) in the pore solution, which may be due to the increased production of N-A-S-H over C-A-S-H. The inclusion of SAP in the pastes resulted in a noticeable reduction in electrical resistivity compared to pastes without SAP. Previous studies have demonstrated that the decrease in electrical resistivity observed in alkali-activated concretes containing SAP may be attributed to a rise in the overall water/binder ratio, leading to an increase in the porosity and a reduction in electrical resistivity [52]. In addition, the electrical resistivity of the pastes is influenced by the saturation degree of macrovoids, as presented in Fig. 4. When the macrovoids are completely saturated, they function as electrical conductors and therefore lower the overall electrical resistivity [52,62].

4.6. Accelerated carbonation Test

Fig. 7 and Fig. 8 show the carbonation depth and photos of the phenolphthalein indicator results for accelerated carbonation of the alkali-activated and OPC/GGBFS concretes. The carbonation depths (Fig. 7) shown are the average values of 15–20 measurements at least 10 mm away from the coated side surface of the samples after 2 and 8 weeks of exposure to 2 % CO_2. Overall, for the alkali-activated concretes both the proportion of precursors, type of alkaline activated and the additions influenced the carbonation mechanism of the samples.

Fig. 7 shows the carbonation depths for the mixes 70CC30S-N, 70CC30S-NS, 70CC30S-NM and 70CC30S-K were respectively, 10.65, 9.88, 10.41 and 11.97 mm at two weeks, indicating an increasing in carbonation depth when KOH was used as activator. After two weeks in exposure to 2 % CO_2, the carbonation depth of the mixes in group 50CC50S followed a similar trend, however a slight decrease was observed for all samples compared to the 70CC30S group. It is worth noting that an exception occurred on the mix with SAP (50CC50S-NS), exhibited a larger depth of carbonation of 10.58 mm when compared to

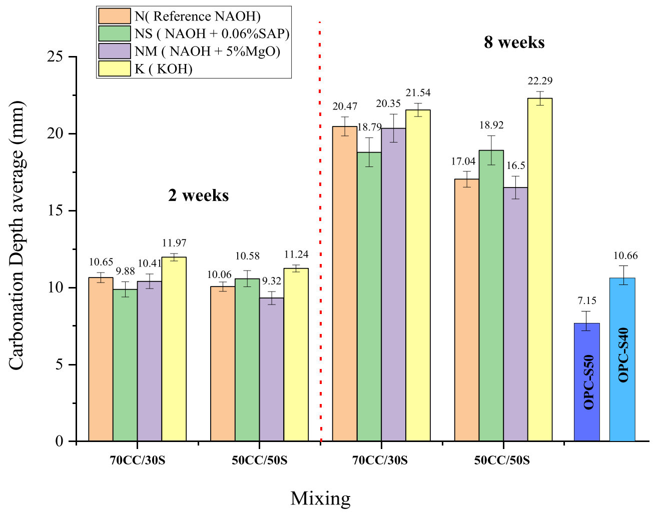

Fig. 7. Average carbonation depth test results after 2 weeks and 8 weeks of AAC mixes.

the composition 70CC30S-NS.

The carbonation depth after 8 weeks of accelerated carbonation exposure is illustrated in Fig. 7. The two concretes with 40 % replacement of OPC by GGBFS showed different carbonation depths. The first one called OPC-S50 (50 MPa grade) had around 7.15 mm carbonation depth after 8 weeks exposed to accelerated carbonation. The second one OPC-S40 (40 MPa grade) had a slightly higher carbonation depth, around 10.66 mm. Regarding the activated alkali concretes, a high carbonation depth was observed. Compared to the two weeks mark, specimens in 70CC30S group exhibited a similar trend after 8 weeks of accelerated carbonation. 70CC30-NS showed the lowest carbonation depth at 18.79 mm while 70CC30-K result slightly increased above (21.54 mm). The substitution in 5 % of GGBFS for MgO in these mixtures did not have a substantial impact, as the values of 70CC30S-N and 70CC30S-NM were comparable up to 8 weeks. High and similar values of carbonation were also observed by Khan and Castel [39] in their research with alkali activated fly ash/GGBFS under accelerated carbonation. For concrete with high GGBFS content (50CC50S), the presence of MgO resulted in the lowest carbonation depth after 2 and 8 weeks of accelerated carbonation exposure. This can be attributed to the lower water absorption and VPV of concrete containing MgO, as shown in Table 3. Additionally, the formation of new crystalline phases when replacing 5 % GGBFS by MgO is discussed in Section 4.7.

The variations on carbonation depth among the different mix designs within the 50CC50S- group after 8 weeks (Fig. 7 and Fig. 8) were similar to those after 2 weeks. The sample denoted as 50CC50S-NM showed the lowest value in terms of penetration depth, whereas the sample activated with KOH (designated as 50CC50S-K) exhibited the highest penetration depth at 15.7 and 22.29 mm respectively (Fig. 7). For the 50CC50S group, the carbonation resistance was enhanced by substituting 5 % MgO (see 50CC50S-NM concrete). This improvement has also been observed in previous studies where the introduction of reactive MgO resulted in the formation of hydrated brucite and hydrotalcite compounds, effectively retarding CO_2 diffusion [50]. Moreover, Zhang et al. [21] observed that the carbonation resistance of alkali-activated mortars incorporating slag as a binder and sodium-containing activators was higher compared to those employing potassium-containing activators. In a previous study by the authors conducted on mortar [20], an important observation was made regarding the impact of GGBFS content on the properties of mortars, due to the presence of Ca-rich phases, such as C-(A)-S-H/C-(N)-A-S-H. These phases act as buffers material and play a crucial role in promoting microstructure densification and enhancing carbonation resistance.

Further investigation is required to ascertain the compatibility of these elevated carbonation depth values with the inherent long-term natural carbonation process of concretes. Additionally, it is important to determine whether if such carbonation levels will lead to the

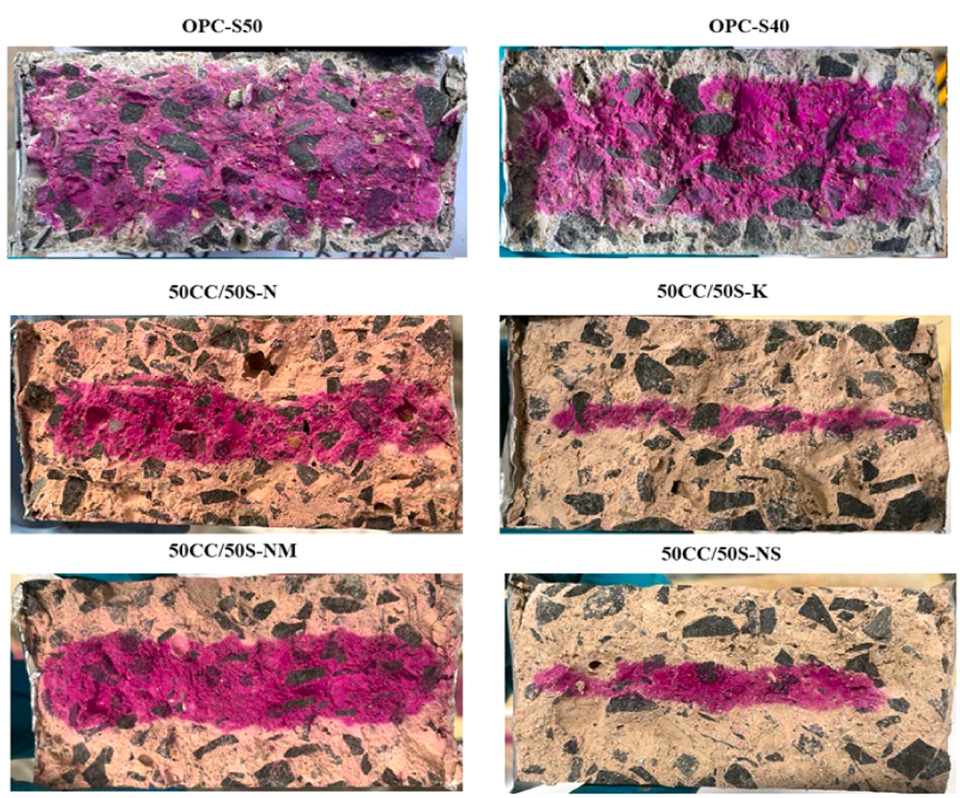

Fig. 8. Phenolphthalein indicator test results exposed to 2 % accelerated carbonation of AAC mixes after 8 weeks.

depassivation of the reinforcement or not. Additional research should be conducted in order to gain a deeper understanding of this phenomenon and its potential implications for structural durability.

4.7. pH measurement of leachate

Fig. 9 shows the pH measurement of leachate results of uncarbonated samples at 28 days and after accelerated carbonation for 8 weeks. For all uncarbonated specimens up to 28 days a pH of 12.36 and above was observed. Mixtures with more percentage of GGBFS (50CC50S group) showed a higher pH value. When incorporating 5 % reactive MgO into the concrete mixes, a slight increase in pH is observed. This effect is more pronounced in samples with higher amounts of GGBFS (50CC50S-NM) compared to 70CC30S-NM. Specifically, at 28 days of age, it was found that the samples labeled as 50CC50S-N exhibited a pH value of 12.63 while those labeled as 50CC50S-NM had a slightly higher value of 12.7. A similar outcome was observed by He et al. [55] with reactive MgO in slag alkali-activated pastes. Furthermore, it is worth noting that the mixtures activated with KOH, 70CC30S-K and 50CC50S-K compositions, displayed a notable decrease in pH levels. The obtained pH values for these mixtures were approximately 12.36 and 12.54 respectively. These pH values were consistent with the highest carbonation depth of mixes containing KOH, as shown in Fig. 7.

In all mixtures, a decrease in pH was observed after exposure to 2 % CO_2 for a period of 8 weeks under accelerated carbonation conditions (Fig. 9). In contrast to the samples that were not subjected to carbonation, it was observed that the samples group 70CC30S exhibited a relatively higher pH compared to their counterparts (50CC50S group) after carbonation. A plausible reason for this phenomenon could be the higher content of GGBFS in 50CC50S group, which leads to a greater presence of C-A-S-H within their microstructure. When exposed to accelerated carbonation, the decalcification of C-A-S-H gels occurs and subsequently gives rise to the formation of calcium carbonates and silica gels. The acidic nature of these newly formed compounds contributes to lowering the pH value. Conversely, N-A-S-H gels remain relatively stable even after undergoing carbonation [63].

In terms of the acceleration of carbonation, it is evident that the pH values remain stable and above the depassivation threshold for steel bars (pH = 9), even after eight weeks exposed to the accelerated carbonation. The pH values are still maintained at approximately 10 or higher in all calcined clay-GGBFS mixtures. Several studies reported that the accelerated carbonation is perhaps not the best approach to evaluate carbonation in alkali-activated materials since the increase in CO_2 in the atmosphere altered the equilibrium of the carbonate phases, leading to reaction products that did not accurately reflect the natural reaction process and also lower the pH to below 10 [16,64]. Further investigation is required under natural and long-term conditions to determine if the substantial carbonation depths and altered pH levels resulting from accelerated carbonation pose a concern for the structural durability of compounds used in construction. Moreover, it is essential to conduct further investigations on reinforcement concrete in order to determine the potential risk of depassivation of steel bars.

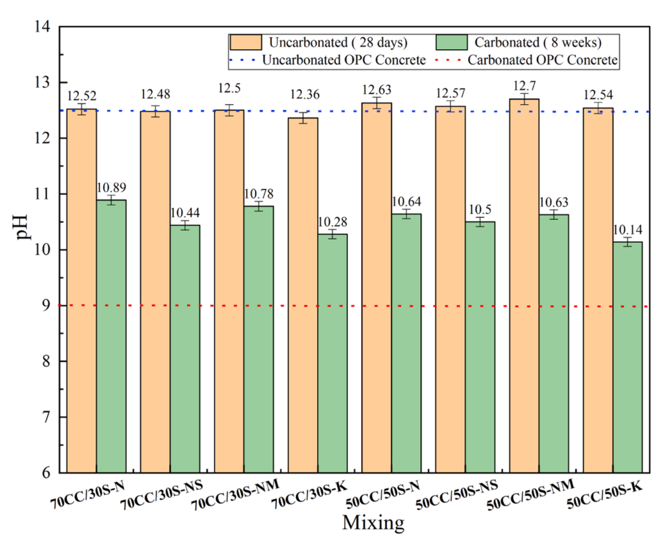

Fig. 9. pH measurement of leachate results of accelerated carbonation of AAC mixes.

4.8. XRD of alkali-activated pastes

Fig. 10 display the X-ray diffraction analyses of uncarbonated alkali-activated pastes containing calcined clay and GBFS after a curing period of 28 days. Quartz (SiO_2) peaks were prominently observed in all crystalline spectra of the mixtures, which can be attributed to the calcined clay as confirmed by XRD measurement on raw calcined clay (Fig. 1). Moreover, it was observed that all of the samples exhibited distinct peaks corresponding to kaolinite at angles of 20.9° 2θ, 39.5° 2θ, and 45.9° 2θ in XRD pattern. Additionally, zeolites from the faujasite family were also detected in the specimens due to the dissolution of metakaolin. For both group of precursor compositions (Fig. 10) the XRD patterns showed a broad diffraction for all the samples around 26° 2θ and 36° 2θ indicating an amorphous phase as the percentage of GGBFS increases to 50 % (Fig. 10 (b)), which is related to C-A-S-H gel formation (26°-36° 2θ). This phenomenon, characterized by the dissolution of calcium hydroxide from GGBFS and the subsequent formation of additional C-A-S-H gel, validating the mechanical results obtained from the group 50CC50S compared to those of 70CC30S group (Fig. 10 (a)). This observation aligns with the previous study of the authors [20].

Overall, for both proportions of precursor (70CC30S-, 50CC50S-), the addition of SAP and the use of KOH did not change the crystalline phase of uncarbonated samples when compared to the specimens activated only with NaOH and sodium silicate (70CC30S-N, 50CC50S-N). However, the replacement of GGBFS by MgO (70CC30S-NM (Fig. 10 (a)), 50CC50S- NM (Fig. 10 (b)) resulted in the appearance of unreacted phases of periclase (MgO) at 42.9° 2θ and peaks of brucite ($Mg(OH)_2$) at 37.0° 2θ and 62.3° 2θ. No trace of hydrotalcite was detected when MgO was added. This is probably due to the low concentration of Mg^{2+} available in the pore solution and excessive silicates available in the system. In a study conducted by Khan & Castel [39], the production of hydrotalcite in systems containing two types of GGBFS and fly ash was investigated. The study reported that despite having a higher concentration of magnesium oxide ranging from 4 % to 9 % by weight, no evidence of hydrotalcite formation was observed. One possible explanation for this finding is that excessive silicates present in the system led to a decrease in the calcium oxide/silicon dioxide ratio. As a result, Mg^{2+} ions may have been incorporated into the C-A-S-H structure rather than being available for hydrotalcite formation within the pore solution. In a study conducted by Suescum-Morales et al. [50], the effects of adding MgO to alkali-activated GGBFS/fly ash systems were investigated. It was determined that the formation of hydrotalcite could not be observed in mixes with an Ms value of 1.5 due to the high silicate modulus. However, brucite phases were detected instead. The volumetric instability of the brucite phases is a result of its expansive reaction products. Although brucite has the capability to fill voids, thereby reducing accessible porosity, it exhibits lower connectivity with its resultant products, which ultimately leads to poorer mechanical performance [50]. This agrees with the results found for the lowest water absorption/VPV (Table 3) and compression strength (Fig. 3) when compared to the samples with only NaOH. Furthermore, this finding may also explain why the inclusion of MgO did not significantly affect the resistance to chloride penetration.

Fig. 11 shows the XRD patterns of carbonated alkali-activated calcined clay and GGBFS mixes after 8 weeks. After the accelerated carbonation process, there is a noticeable rise in calcite and C-(A)-S-H

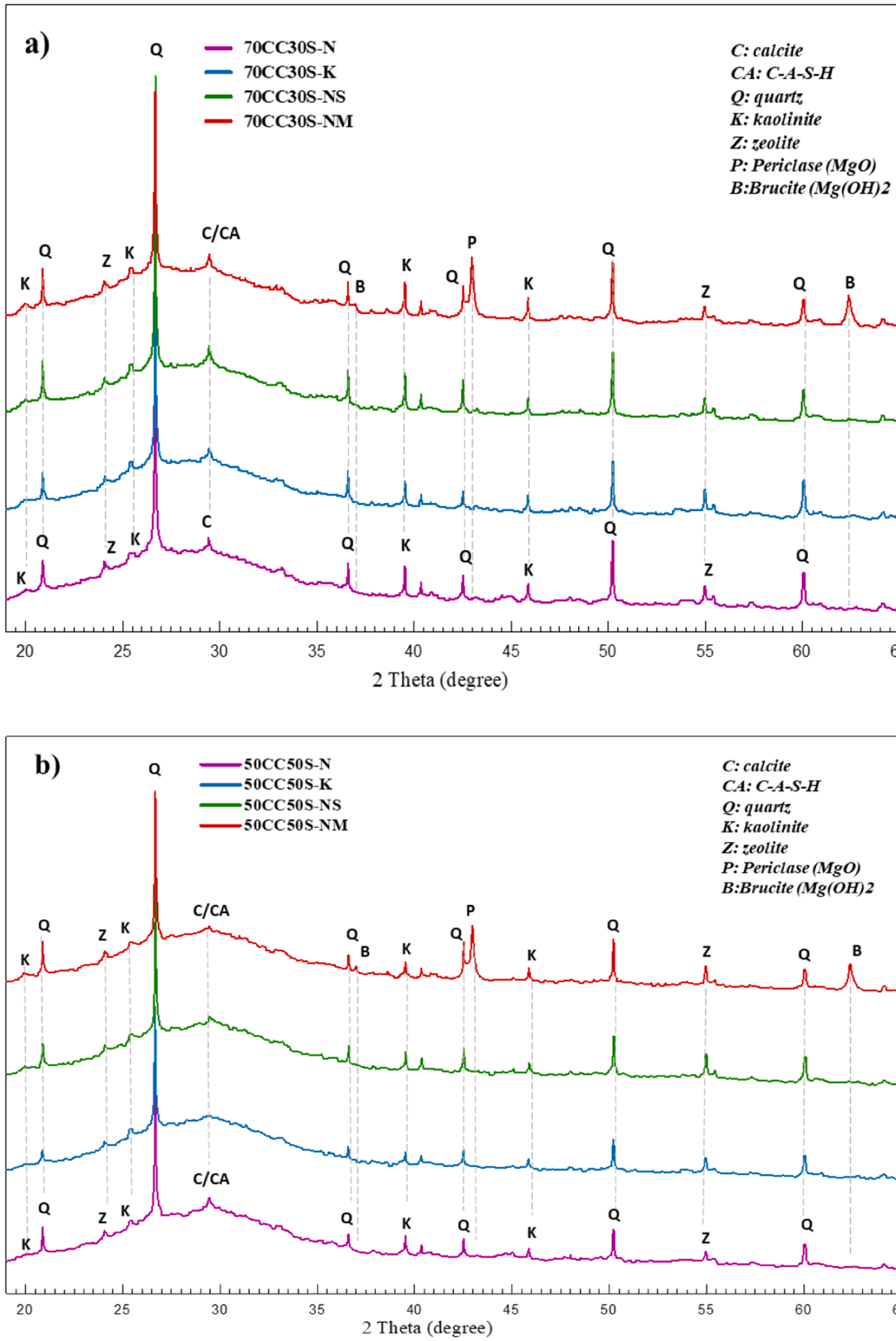

Fig. 10. XRD diffractograms of uncarbonated alkali-activated calcined clay/GGBFS (a) 70 %Calcined clay (b) 50 % Calcined clay.

peak. Additionally, calcium carbonate polymorph phases like aragonite ($CaCO_3$) and vaterite ($CaCO_3$) become visible. Furthermore, due to the accelerated carbonation process, peaks corresponding to sodium bicarbonate compounds such as Nahcolite ($NaHCO_3$) were detected. Additionally, the appearance of Gaylussite ($Na_2Ca(CO_3)$, a sodium-calcium carbonate compound, was also observed and was directly linked to the carbonation occurring in the pore solution.

As observed in Fig. 11,both groups labeled as 70CC30S (Fig. 11(a)) and 50CC50S (Fig. 11(b)) exhibited peaks indicating the decalcification of the C-A-S-H phase. These peaks were attributed to aragonite at angles of 26.2° 2θ and 52.5° 2θ, as well as vaterite at an angle of 27.2° 2θ and calcite overlapping C-A-S-H peak at 29.5° 2θ. The presence of these peaks was more pronounced in the groups with higher GGBFS and calcium content (50CC50S). Previous research on alkali-activated GGBFS [27] has shown similar findings, supporting the notion that the formation of $CaCO_3$ during accelerated carbonation follows an Ostwald-type mechanism. This process involves the crystallization of the least stable polymorph of $CaCO_3$ and simultaneously there is also the generation of hydrous sodium carbonates phases of pore solution [21,27]. Gaylussite (33.2° 2θ) and Nahcolite (36.1° 2θ) were detected in almost all samples, but with less intensity in 70CC30S group with higher amounts of calcined clay (Fig. 11(a)). This can be attributed to less available Na^+ ions in the pore solution of 70CC30S group than that of 50CC50S group. The results are consistent with the outcomes from the 50CC50S groups

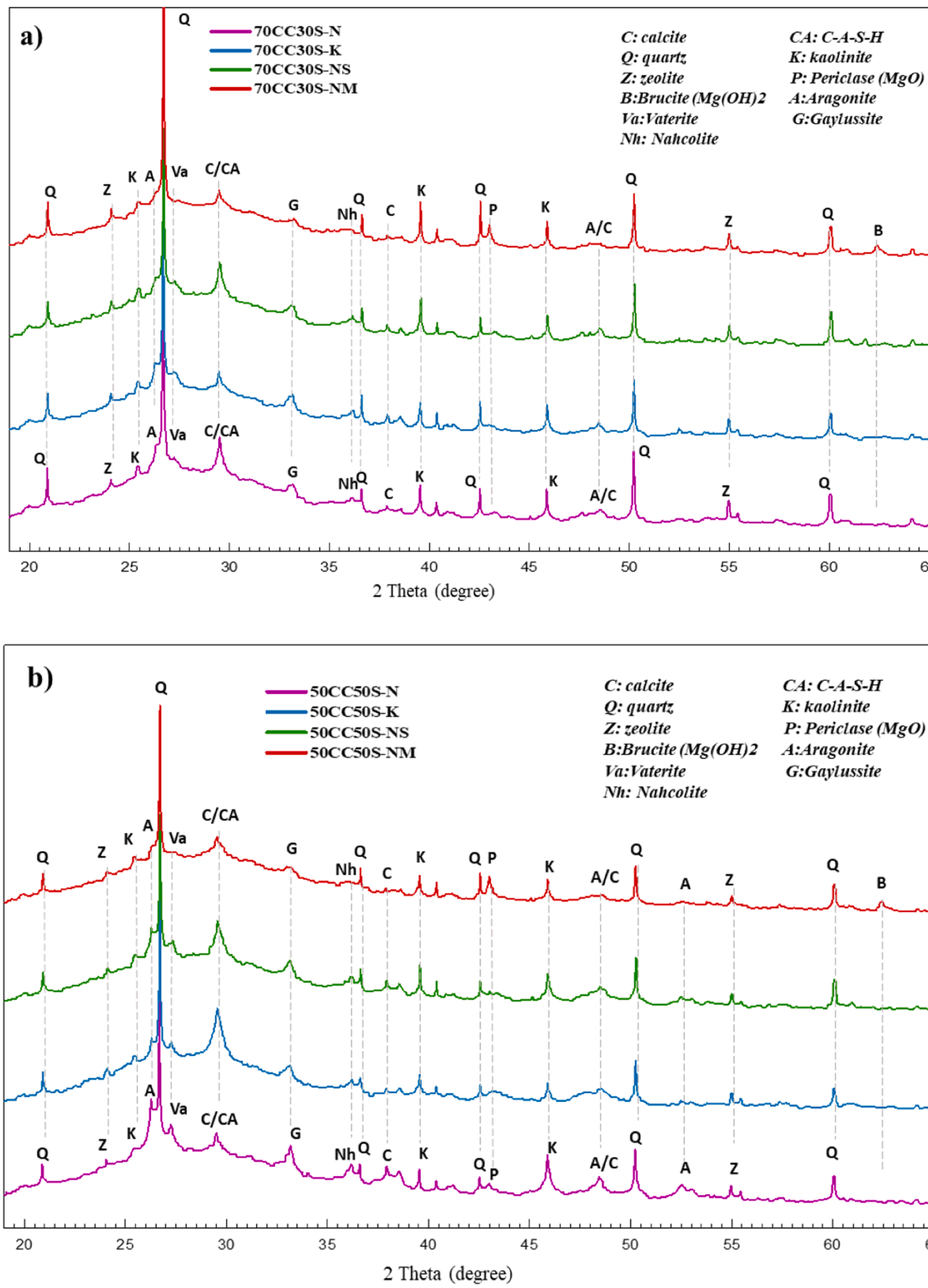

Fig. 11. XRD diffractograms of 8-week carbonated alkali-activated calcined clay/GGBFS (a) 70CC30S-group (b) 50CC50S-group.

in terms of carbonation depth. These groups demonstrated a reduced extent of carbonation due to an increased presence of C-A-S-H (also showed in the previous study of the authors [20]), which acted as a barrier for CO_2 diffusion before its decalcification. Additionally, there was probably an elevated concentration of Na^+ ions available in the pore solution of 50CC50S group compared to the groups 70CC30S (in agreement with RCPT and surface/bulk resistivity results), which also retards the carbonation diffusion as it is also reacts with CO_2, resulting in higher peaks of hydrous sodium carbonate (Gaylussite) and bicarbonate (Nahcolite) for the 50CC50S group. The lower pH (Fig. 9) observed in the samples from the 50CC50S group (Fig. 11(b)) after accelerated carbonation may be attributed to a higher formation of these crystalline phases compared to the samples from the 70CC30S group (Fig. 11(a)). It was observed that the introduction of SAP and substitution of NaOH with KOH did not result in any noticeable alterations in the crystalline phases among all groups. This finding implies that regardless of whether SAP or KOH were included, they resulted in the same decalcification of the C-A-S-H and peaks of sodium carbonates phases.

After being subjected to accelerated carbonation, the inclusion of MgO led to significant changes in the crystalline phases. It is apparent from the results that the presence of MgO caused a decrease in both C-A-S-H decomposition-related peaks and those associated with pore solution for all experimental groups (Fig. 11). Fig. 12 shows the comparison between samples 50CC50S-N and 50CC50S-NM before and after accelerated carbonation. The presence of MgO was found to significantly decrease the intensity and quantity of the peaks associated with carbonation products formed from the pore solution, which is probably associated with a lower concentration of free Na^+ in the pore solution which agrees with the results of RCPT test. Additionally, it also reduced the calcium carbonates phases. Fig. 12 shows the calcite, aragonite and vaterite peaks decreasing its intensity or not being detected in the carbonated samples with the presence of MgO (50CC50S-NM).

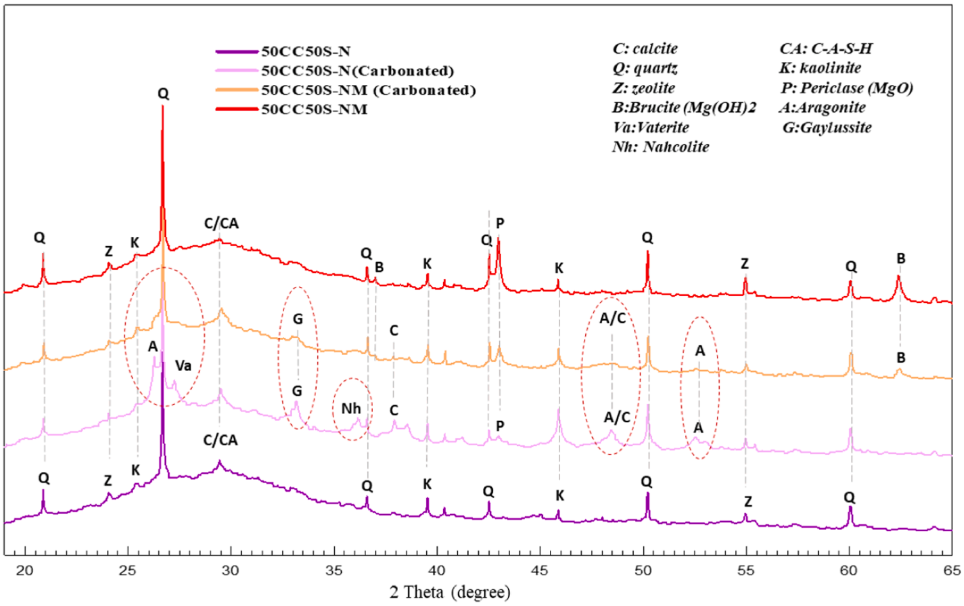

Fig. 12. Comparative of carbonated and uncarbonated 50CC50S- group with and without MgO.

Furthermore, the intensities of peaks associated with pore solution carbonation, such as Gaylussite ($Na_2Ca_2{\cdot}5\,H_2O$), were significantly reduced or completely absent in samples containing MgO. This was also observed for Nahcolite ($NaHCO_3$) at 36.1° 2θ. Moreover, the presence of peaks associated with magnesium oxide compounds such as periclase and brucite exhibited a decrease or complete disappearance, particularly in the case of the latter. The carbonation of these two phases in the form of $MgCO_3$ may be linked to this phenomenon. These findings align with the evidence suggesting that the inclusion of MgO in calcined clay-GGBFS alkali-activated systems can effectively mitigate carbonation as presented in Fig. 7. The buffering properties of MgO phases, such as periclase and brucite, contributed to this mitigation effect. This is similar to the role played by $Ca(OH)_2$ in conventional OPC systems [25]. Small diffraction peaks of $MgCO_3$ were observed in the samples without additional MgO (50CC50S-N) after carbonation at a 42.9° 2θ angle. This can be attributed to the carbonation of MgO in the GGBFS, which has a magnesium oxide content of 4.62 wt% as detected by XRF (Table 1). Park et al. [25] conducted a study investigating the function of MgO as a buffering system to minimize the decomposition of C-A-S-H. The findings indicated that even unhydrated MgO presents in the slurry could undergo direct carbonation, resulting in the formation of both magnesium carbonate and hydrated form of magnesium carbonate (hydrate-$MgCO_3$). As a result, this process resulted in an increase in volume and hindered CO_2 diffusion.

5. Conclusions

The experimental investigation conducted aimed to assess the effects of different mix components on the mechanical, physical and durability properties of alkali-activated concretes containing a low-grade calcined clay and ground granulated blast furnace slag (GGBFS), different activators such as NaOH/KOH and additives like MgO and SAP. The primary focus was on analyzing the physical-mechanical characteristics of these composites, specifically their performance under accelerated carbonation conditions and chloride diffusion. Through this analysis, several conclusions were drawn regarding the response of these materials to these degradation mechanisms:

(1) In terms of the compressive strength of concrete, calcined clay-GGBFS geopolymer concretes achieved average compressive strength ranging from 41.2 to 53.3 MPa, which makes them suitable for most structural applications, including severe environments. However, based on the modified-RCPT (10 V) and NT Build 492 results and correlations, all concretes were classified as "High Chloride penetrability" due to its value being higher than 350 coulombs for the modified-RCPT (10 V) and 13.5 ($\times 10^{-12}$ m^2/s) for the non-steady-state migration coefficient (D_{nssm}), thus not recommended for chloride environments.

(2) The composition ratio of GGBFS in the mixtures played a pivotal role. Except for the SAP specimens, the increasing in GGBFS led to a reduction in water and volume of permeable voids (VPV) results. For the modified-RCPT (10 V), the group with the highest proportion of GGBFS (50CC50S) recorded higher values compared to the 70CC30S mixes. However, the opposite was noted in the rapid migration test (RMT) - NT Build 492. Among all the specimens, the most favorable outcome was achieved by the mix with 50 % GGBFS (50CC50S-N), which recorded a non-steady-state migration coefficient (D_{nssm}) value around 55.68 ($\times 10^{-12}$ m^2/s).

(3) The surface and bulk resistivity analysis showed that mixtures composed of 70 % calcined clay and 30 % GGBFS outperformed those with 50CC50S composition, with SAP mixtures being the only exception. The enhanced performance is likely attributed to the decrease in free sodium ions (Na^+) in the pore solution of the 70CC30S mixture group, as a result of N-A-S-H formation over C-A-S-H.

(4) During the accelerated carbonation tests, the 50CC50S group displayed the lowest carbonation depth. However, the 70CC30S mix maintained a slightly higher pH than the 50CC50S group. This can be linked to the increased production reaction of $CaCO_3$, sodium carbonate phases in the highest GGBFS percentage group (50CC50S), suggesting a higher free Na^+ presence in its pore solution, leading to a more pronounced pH drop post-carbonation, corroborated by XRD findings.

(5) Regarding the alkaline activator, employing NaOH combined with sodium silicate as an alkali activator resulted in superior compressive strength when contrasted with the combination of KOH and sodium silicate. Specimens activated with KOH displayed the highest carbonation depth after 8 weeks exposed to the high CO_2 atmosphere, with measurements of 21.54 mm and 22.29 mm for the 70CC30S and 50CC50S groups, respectively.

(6) Incorporating 0.6 % superabsorbent polymer (SAP) into the concrete led to a reduction in its compressive strength. Samples containing SAP, specifically 70CC30S-NS and 50CC/50S-NS, showed a slight increase in water absorption, recording values of about 7.79 % and 8.44 % respectively. Interestingly, the addition of 0.6 % SAP to the 70CC30S-NS composition led to a favorable effect in the non-steady-state migration coefficient. This specific blend experienced a reduction of 20.4 % in the D_{nssm} value compared to the 70CC30S-N concrete.

(7) The specimens containing magnesium oxide, specifically the 70CC30S-NM and 50CC/50S-NM compositions, displayed the lowest levels of water absorption. These particular specimens exhibited water absorption values of only 6.9 % and 6.6 %, respectively. In the context of accelerated carbonation, the sample with highest proportion of GGBFS and 5 % replacement by MgO (referred to as 50CC50S-NM), exhibited the lowest carbonation depth at 15.7 mm. The occurrence of magnesium-bearing phases, as evidenced by XRD analysis, in conjunction with the residual presence of magnesium oxide served as a chemical buffering mechanism that inhibited the degree of carbonation. The existence of periclase and brucite resulted in a reduction in calcium carbonate phases (such as calcite, aragonite, and vaterite) and minimized peaks associated with carbonation related to pore solution such as gaylussite and nahcolite.

CRediT authorship contribution statement

Samuel De Carvalho Gomes: Conceptualization, Methodology, Validation, Formal analysis, Investigation, Data curation, Writing – original draft, Visualization. **Quang Dieu Nguyen:** Conceptualization, Methodology, Validation, Formal analysis, Investigation, Writing – review & editing, Supervision. **Wengui Li:** Investigation, Writing – review & editing, Supervision. **Arnaud Castel:** Conceptualization, Methodology, Validation, Resources, Writing – review & editing, Supervision, Project administration, Funding acquisition.

Declaration of Competing Interest

The authors declare that they have no known competing financial interests or personal relationships that could have appeared to influence the work reported in this paper.

Acknowledgements

The authors would like to thank the School of Civil and Environmental Engineering, University of Technology Sydney (UTS) - Tech Lab, Sydney, NSW for providing technical support.

Data Availability

Data will be made available on request.

References

[1] L. Barcelo, J. Kline, G. Walenta, E. Gartner, Cement and carbon emissions, Mater. Struct. 47 (2013) 1055–1065.

[2] W. Sae-Long, T. Chompoorat, S. Limkatanyu, N. Damrongwiriyanupap, P. Sukontasukkul, T. Chub-Uppakarn, T. Thepumong, Experimental and simulation analysis of RCA and para-wood ash as partial substitutes for NCA and cement in recycled aggregate concrete, Case Stud. Constr. Mater. 21 (2024) e03716.

[3] T. Chub-uppakarn, T. Chompoorat, T. Thepumong, W. Sae-Long, A. Khamplod, S. Chaiprapat, Influence of partial substitution of metakaolin by palm oil fuel ash and alumina waste ash on compressive strength and microstructure in metakaolin-based geopolymer mortar, Case Stud. Constr. Mater. 19 (2023) e02519.

[4] B. Singh, G. Ishwarya, M. Gupta, S.K. Bhattacharyya, Geopolymer concrete: a review of some recent developments, Constr. Build. Mater. 85 (2015) 78–90.

[5] J.L. Provis, Geopolymers and other alkali activated materials: why, how, and what? Mater. Struct. 47 (2014) 11–25.

[6] F. Farooq, X. Jin, M. Faisal Javed, A. Akbar, M. Izhar Shah, F. Aslam, R. Alyousef, Geopolymer concrete as sustainable material: a state of the art review, Constr. Build. Mater. 306 (2021) 124762.

[7] S.O. Sore, A. Messan, E. Prud'Homme, G. Escadeillas, F. Tsobnang, Comparative study on geopolymer binders based on two alkaline solutions (NaOH and KOH), J. Miner. Mater. Charact. Eng. 08 (2020) 407–420.

[8] B.B. Jindal, T. Alomayri, A. Hasan, C.R. Kaze, Geopolymer concrete with metakaolin for sustainability: a comprehensive review on raw material's properties, synthesis, performance, and potential application, Environ. Sci. Pollut. Res Int 30 (2023) 25299–25324.

[9] A.M. Okashah, F.F. Zainal, N.F. Hayazi, M.N. Nordin, A. Abdullah, Pozzolanic properties of calcined clay in geopolymer concrete: a review, AIP Conf. Proc. 2339 (2021).

[10] S. Krishnan, G.R. Dhoopadahailli, S. Bishnoi, Why Low-Grade Calcined Clays are Ideal for the Production of Limestone Calcined Clay Cement (LC3), 3rd International Conference on Calcined Clays for Sustainable Concrete, 2019, pp. 115-120.

[11] B. Ayati, D. Newport, H. Wong, C. Cheeseman, Low-carbon cements: Potential for low-grade calcined clays to form supplementary cementitious materials, Cleaner, Materials 5 (2022) 100099.

[12] Q.D. Nguyen, S. Afroz, A. Castel, Influence of calcined clay reactivity on the mechanical properties and chloride diffusion resistance of limestone calcined clay cement (LC3) concrete, J. Mar. Sci. Eng. 8 (2020) 301.

[13] A. Alujas Diaz, R.S. Almenares Reyes, T. Hanein, E.F. Irassar, M. Juenger, F. Kanavaris, M. Maier, A.T. Marsh, T. Sui, K.-C. Thienel, L. Valentini, B. Wang, F. Zunino, R. Snellings, Properties and occurrence of clay resources for use as supplementary cementitious materials: a paper of RILEM TC 282-CCL, Mater. Struct. 55 (2022) 139.

[14] S. Afroz, Y. Zhang, Q.D. Nguyen, T. Kim, A. Castel, Shrinkage of blended cement concrete with fly ash or limestone calcined clay, Mater. Struct. 56 (2023) 15.

[15] A.S. Bature, M. Khorami, E. Ganjian, M. Tyrer, Influence of alkali activator type and proportion on strength performance of calcined clay geopolymer mortar, Constr. Build. Mater. 267 (2021) 120446.

[16] S.A. Bernal, R. Mejía de Gutiérrez, J.L. Provis, Engineering and durability properties of concretes based on alkali-activated granulated blast furnace slag/metakaolin blends, Constr. Build. Mater. 33 (2012) 99–108.

[17] N.R. Rakhimova, V.P. Morozov, A.A. Eskin, Y.S. Lutskin, O.S. Shynkevych, Blended alkali-activated cements based on blast-furnace slag and calcined clays: statistical modeling and effect of amount and chemistry of reactive phase, J. Mater. Civ. Eng. 34 (2022) 04022112.

[18] K.M.L. Alventosa, C.E. White, The effects of calcium hydroxide and activator chemistry on alkali-activated metakaolin pastes, Cem. Concr. Res. 145 (2021) 106453.

[19] H. Peng, C. Cui, Z. Liu, C.S. Cai, Y. Liu, Synthesis and reaction mechanism of an alkali-activated metakaolin-slag composite system at room temperature, J. Mater. Civ. Eng. 31 (2019) 04018345.

[20] S.D.C. Gomes, Q.D. Nguyen, W. Li, A. Castel, Carbonation resistance of calcined clay-ground granulated blast furnace slag alkali-activated mortar, Constr. Build. Mater. 393 (2023) 131811.

[21] X. Zhang, K. Long, W. Liu, L. Li, W.J. Long, Carbonation and chloride ions' penetration of alkali-activated materials: a review, Molecules 25 (2020) 5074.

[22] X. Ke, S.A. Bernal, J.L. Provis, Uptake of chloride and carbonate by Mg-Al and Ca-Al layered double hydroxides in simulated pore solutions of alkali-activated slag cement, Cem. Concr. Res. 100 (2017) 1–13.

[23] O.A. Mohamed, A Review of Durability and Strength Characteristics of Alkali-Activated Slag Concrete, Mater. (Basel) 12 (2019) 1198.

[24] M.S.H. Khan, O. Kayali, U. Troitzsch, Chloride binding capacity of hydrotalcite and the competition with carbonates in ground granulated blast furnace slag concrete, Mater. Struct. 49 (2016) 4609–4619.

[25] H.N. Yoon, S.M. Park, H.K. Lee, Effect of MgO on chloride penetration resistance of alkali-activated binder, Constr. Build. Mater. 178 (2018) 584–592.

[26] B. Akturk, M. Abolfathi, S. Ulukaya, A.B. Kizilkanat, T.J.N. Hooper, L. Gu, E.-H. Yang, C. Unluer, Hydration kinetics and performance of sodium carbonate-activated slag-based systems containing reactive MgO and metakaolin under carbonation, Cem. Concr. Compos. 132 (2022) 104617.

[27] S.A. Bernal, R. San Nicolas, R.J. Myers, R. Mejía de Gutiérrez, F. Puertas, J.S.J. van Deventer, J.L. Provis, MgO content of slag controls phase evolution and structural changes induced by accelerated carbonation in alkali-activated binders, Cem. Concr. Res. 57 (2014) 33–43.

[28] S.Y. Wang, E. McCaslin, C.E. White, Effects of magnesium content and carbonation on the multiscale pore structure of alkali-activated slags, Cem. Concr. Res. 130 (2020) 105979.

[29] N.K. Lee, K.T. Koh, M.O. Kim, G.H. An, G.S. Ryu, Physicochemical changes caused by reactive MgO in alkali-activated fly ash/slag blends under accelerated carbonation, Ceram. Int. 43 (2017) 12490–12496.

[30] S. Afridi, M.A. Sikandar, M. Waseem, H. Nasir, A. Naseer, Chemical durability of superabsorbent polymer (SAP) based geopolymer mortars (GPMs), Constr. Build. Mater. 217 (2019) 530–542.

[31] W. Al Makhadmeh, A. Soliman, Understanding the shrinkage behaviour of alkali-activated slag binders modified by the superabsorbent polymer, Constr. Build. Mater. 365 (2023) 130053.

[32] ASTM, ASTM C39/C39M-18: Standard Test Method for Compressive Strength of Cylindrical Concrete Specimens, ASTM International, West Conshohocken, PA, 2018.

[33] A. Noushini, A. Castel, The effect of heat-curing on transport properties of low-calcium fly ash-based geopolymer concrete, Constr. Build. Mater. 112 (2016) 464–477.
[34] ASTM C642-13: Standard Test Method for Density, Absorption, and Voids in Hardened Concrete, ASTM International, West Conshohocken, PA, 2013.
[35] A. Noushini, A. Castel, Performance-based criteria to assess the suitability of geopolymer concrete in marine environments using modified ASTM C1202 and ASTM C1556 methods, Mater. Struct. 51 (2018) 146.
[36] ASTM C1012/C1012M: Standard Test Method for Length Change of Hydraulic-Cement Mortars Exposed to a Sulfate Solution, ASTM International, West Conshohocken, PA, 2018.
[37] Nordtest, N.T. Build 492 (1999-11): Concrete, mortar and cement-based repair materials: chloride migration coefficient from non-steady-state migration experiments, Nordtest, Finland, 1999.
[38] Q.D. Nguyen, M.S.H. Khan, A. Castel, T. Kim, Durability and Microstructure Properties of Low-Carbon Concrete Incorporating Ferronickel Slag Sand and Fly Ash, J. Mater. Civ. Eng. 31 (2019) 04019152.
[39] M.S.H. Khan, A. Castel, Effect of MgO and Na2SiO3 on the carbonation resistance of alkali activated slag concrete, Mag. Concr. Res. 70 (2018) 685–692.
[40] M.S.H. Khan, Q.D. Nguyen, A. Castel, Performance of limestone calcined clay blended cement-based concrete against carbonation, Adv. Cem. Res. 32 (2020) 481–491.
[41] AS, AS 3600: Concrete structures, Standards Australia, Sydney, Australia, 2018.
[42] AS, AS 5100.5: Bridge design Part 5: Concrete, Standards Australia, Sydney, Australia, 2017.
[43] I. Nikolic, M. Tadic, I. Jankovic-Castvan, V. Radmilovic, V. Radmilovic, Durability of alkali activated slag in a marine environment: Influence of alkali ion, J. Serb. Chem. Soc. 83 (2018) 1143–1156.
[44] A. Poulesquen, F. Frizon, D. Lambertin, Rheological behavior of alkali-activated metakaolin during geopolymerization, J. Non-Cryst. Solids 357 (2011) 3565–3571.
[45] S. Moradikhou, A.B. Moradikhou, Geopolymer concrete based on class c fly ash cured at ambient condition, J. Civ. Eng. Mater. Appl. 5 (2021) 177–195.
[46] H. Xu, J.S.J. Van Deventer, The geopolymerisation of alumino-silicate minerals, Int. J. Miner. Process. 59 (2000) 247–266.
[47] P. Duxson, S.W. Mallicoat, G.C. Lukey, W.M. Kriven, J.S.J. van Deventer, The effect of alkali and Si/Al ratio on the development of mechanical properties of metakaolin-based geopolymers, Colloids Surf. A: Physicochem. Eng. Asp. 292 (2007) 8–20.
[48] A. Palomo, A. Fernández-Jiménez, M. Criado, Activación alcalina de cenizas volantes, Estud. Comp. entre Act. S. ódicos Y. potásicos, Mater. Construcc 56 (2008) 51–65.
[49] Y. Luna-Galiano, C. Fernández-Pereira, M. Izquierdo, Contributions to the study of porosity in fly ash-based geopolymers. Relationship between degree of reaction, porosity and compressive strength, Mater. Construcc 66 (2016) e098.
[50] D. Suescum-Morales, M. Bravo, R.V. Silva, J.R. Jiménez, J.M. Fernandez-Rodriguez, J. de Brito, Effect of reactive magnesium oxide in alkali-activated fly ash mortars exposed to accelerated CO2 curing, Constr. Build. Mater. 342 (2022) 127999.
[51] W. Tu, Y. Zhu, G. Fang, X. Wang, M. Zhang, Internal curing of alkali-activated fly ash-slag pastes using superabsorbent polymer, Cem. Concr. Res. 116 (2019) 179–190.
[52] B. Vafaei, K. Farzanian, A. Ghahremaninezhad, The influence of superabsorbent polymer on the properties of alkali-activated slag pastes, Constr. Build. Mater. 236 (2020) 117525.
[53] K. Farzanian, K. Pimenta Teixeira, I. Perdigão Rocha, L. De Sa Carneiro, A. Ghahremaninezhad, The mechanical strength, degree of hydration, and electrical resistivity of cement pastes modified with superabsorbent polymers, Constr. Build. Mater. 109 (2016) 156–165.
[54] A. Pourjavadi, S.M. Fakoorpoor, P. Hosseini, A. Khaloo, Interactions between superabsorbent polymers and cement-based composites incorporating colloidal silica nanoparticles, Cem. Concr. Compos. 37 (2013) 196–204.
[55] J. He, W. Zheng, W. Bai, T. Hu, J. He, X. Song, Effect of reactive MgO on hydration and properties of alkali-activated slag pastes with different activators, Constr. Build. Mater. 271 (2021) 121608.
[56] C. Unluer, A. Al-Tabbaa, Impact of hydrated magnesium carbonate additives on the carbonation of reactive MgO cements, Cem. Concr. Res. 54 (2013) 87–97.
[57] ASTM, ASTM C1556-11a (2016): Standard Test Method for Determining the Apparent Chloride Diffusion Coefficient of Cementitious Mixtures by Bulk Diffusion, ASTM International, West Conshohocken, PA, 2016.
[58] ASTM C1202-17a: Standard Test Method for Electrical Indication of Concrete's Ability to Resist Chloride Ion Penetration, ASTM International, West Conshohocken, PA, 2017.
[59] J. Zhang, Y. Ma, J. Hu, H. Wang, Z. Zhang, Review on chloride transport in alkali-activated materials: role of precursors, activators and admixtures, Constr. Build. Mater. 328 (2022) 127081.
[60] A. Noushini, Q.D. Nguyen, A. Castel, Assessing alkali-activated concrete performance in chloride environments using NT Build 492, Mater. Struct. 54 (2021) 57.
[61] H. Alanazi, J. Hu, Y.-R. Kim, Effect of slag, silica fume, and metakaolin on properties and performance of alkali-activated fly ash cured at ambient temperature, Constr. Build. Mater. 197 (2019) 747–756.
[62] H.S. Wong, A.M. Pappas, R.W. Zimmerman, N.R. Buenfeld, Effect of entrained air voids on the microstructure and mass transport properties of concrete, Cem. Concr. Res. 41 (2011) 1067–1077.
[63] J. Zhang, C. Shi, Z. Zhang, Carbonation induced phase evolution in alkali-activated slag/fly ash cements: The effect of silicate modulus of activators, Constr. Build. Mater. 223 (2019) 566–582.
[64] R. Pouhet, M. Cyr, Formulation and performance of flash metakaolin geopolymer concretes, Constr. Build. Mater. 120 (2016) 150–160.